International Journal of Nanomedicine

Dovepress
open access to scientific and medical research

Open Access Full Text Article

ORIGINAL RESEARCH

RETRACTED ARTICLE: Preparation, Pharmacokinetics, and Antitumor Potential of Miltefosine-Loaded Nanostructured Lipid Carriers

Guo Yu[1]
Zakir Ali[2]
Anam Sajjad Khan[2]
Kalim Ullah[3]
Humzah Jamshaid[2]
Alam Zeb[4]
Muhammad Imran[4]
Sadia Sarwar[4]
Han-Gon Choi[5]
Fakhar ud Din[2]

[1]Department of Head and Neck Breast, Xinxiang Central Hospital, The Fourth Clinical College of Xinxiang Medical University, Xinxiang City, Henan Province, 453000, People's Republic of China; [2]Nanomedicine Research Group, Department of Pharmacy, Faculty of Biological Sciences, Quaid-i-Azam University, Islamabad, 45320, Pakista[3]Department of Zoology, Kohat University of Science & Technology, Koha Khyber Pakhtunkhwa, Pakistan; [4]Ri an Institute of Pharmaceutical Sciences phah International University, mabad akistan; [5]College of Pharmacy & Ins of Pharmaceutical and Te ology, Hanyang U rsity, A an, South

Correspondence: Fakhar ud Din
Tel +92 512-90644314
Fax +92 512-90644144
Email fudin@qau.edu.pk

Han-Gon Choi
Email hangon@hanyang.ac.kr

Received: 28 December 2020
Accepted: 7 April 2021
Published: 11 May 2021

Background: The purpose of this study was to i estigate the su ili of nanostructured lipid carriers (NLCs) loaded with miltefosine (H C) as a anticancer drug for the treatment of breast cancer.

Methods: HePC-NLCs were prepared g a microe lsio echnique and then evaluated for particle size, polydispersity in x (PD incorporati efficiency, in vitro release of entrapped drug, and hemolytic potential. Furth ore, pharmacokinetic, biodistribution, and liver toxicity analyses were rformed in Sprague awley rats, and antitumor efficacy was evaluated in Michigan Can r Foundation 7 (MCF-7) and squamous cell carcinoma-7 (SCC-7) cells in vitro and in tum r-bearing B B/c mice in vivo. Advanced analyses including survival rate, immunohistopa logy, an terminal deoxynucleotidyl transferase dUTP nick end labelling (T NE ssays were performed to evaluate apoptosis in vivo.

Results: The aver e par e of the HePC-NLCs was 143 ± 16 nm, with a narrow PDI (0.104 0.002), a e incorporation efficiency was found to be 91 ± 7%. The NLCs rele ed He in a s tained manner, and this release was significantly lower than that of f e drug. e in vitr hemolytic assay demonstrated a significantly reduced hemolytic pote ial (~9%) of the NLCs compared to that of the test formulations. The HePC-NLCs demons ted enhanced pharmacokinetic behaviour over free drug, including extended blood circulation d an abridged clearance rate in rats. Furthermore, the HePC-NLCs exhibited gher cytotoxicity than the free drug in MCF-7 and SCC-7 cells. Moreover, the HePC-NLCs sho d significantly enhanced ($P < 0.005$) antitumor activity compared to that of the control and free drug-treated mouse groups. Tumour cell apoptosis was also confirmed, indicating the antitumor potential of the HePC-NLCs.

Conclusion: These findings demonstrate the ability of NLCs as a drug delivery system for enhanced pharmacokinetic, antitumor, and apoptotic effects, most importantly when loaded with HePC.

Keywords: breast cancer, miltefosine, nano lipid carriers, bioavailability, pharmacokinetics, antitumor efficacy

Introduction

Cancer is the second leading cause of death globally. According to the International Agency for Research on Cancer and the World Health Organization, 18.1 million new cases of cancer and 9.6 million deaths were reported in 2018.[1] The hallmarks of tumour progression are cell expansion and metastasis. Thus, novel anticancer agents have been loaded into various nanocarriers to inhibit tumour cell

proliferation and tumour progression.[2] Some of these agents include docetaxel,[3] irinotecan,[4] doxorubicin,[5] methotrexate,[6] and miltefosine.[7] Miltefosine, also known as hexadecylphosphocholine (HePC), is a synthetic alkyl phospholipid that represents a new class of drug with antiproliferative properties against tumour cells. Although HePC has been used as an antileishmanial agent, it has also been investigated for its promising therapeutic anticancer effects.[8] Unlike classical anticancer agents, which kill tumour cells by interrupting DNA replication, HePC induces apoptosis of tumour cells by targeting the plasma membrane. The structural similarity of HePC with membrane lipids facilitates its insertion into lipid bilayers. Following membrane incorporation, the metabolically active drug interferes with several critical membrane functions, importantly, phospholipid biosynthesis and phospholipid-mediated signal transduction pathways[9] (Figure 1A and B). HePC primarily impedes phosphatidylcholine (PC) turnover, a chief component of the cell membrane, as well as lipid-mediated intracellular signalling pathways. The inhibition of cytidylyltransferase is responsible for this reduced PC level (Figure 1C). This is coupled with the inhibition of phospholipase C (PLC), another important enzyme in phospholipid-mediated signal transduction pathways. PLC inhibition attenuates production of the second messengers, diacylglycerol (DAG) and inositol 1,4,5-trisphosphate (IP_3), which in turn blocks the intracellular survival pathway involving phosphoinositide 3-kinase (PI3K)/protein kinase B (PKB) signalling (Figure 1D). Another prominent action of HePC is the

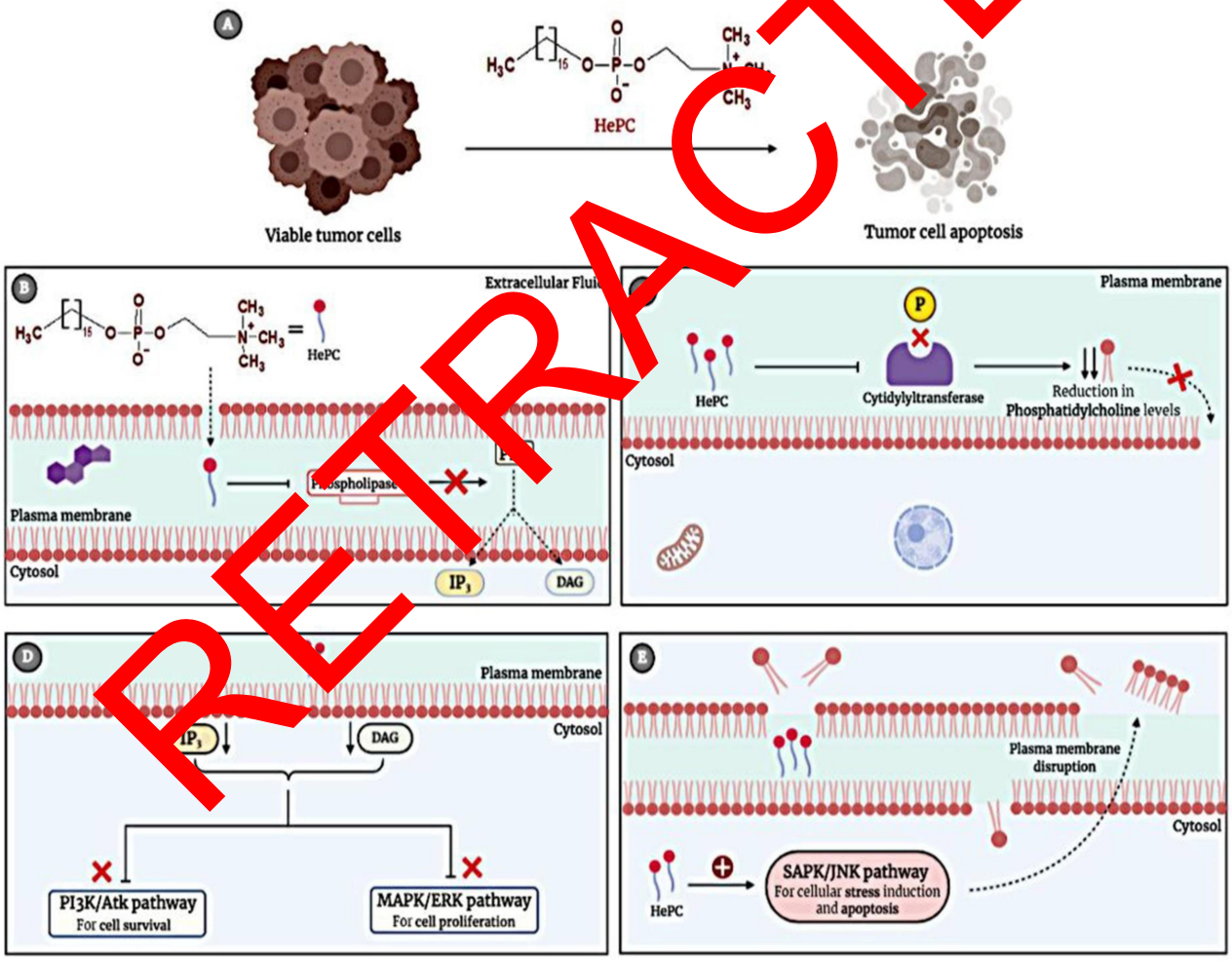

Figure 1 Representative diagram of mechanisms of action of HePC. (**A**) Chemical structure of HePC and HePC-mediated tumour cell apoptosis. (**B**) Incorporation of HePC inside plasma membrane lipid bilayers and HePC-mediated phospholipase C inhibition and downregulation of phosphatidylinositol 4,5-bisphosphate (PIP_2) conversion into IP_3 and DAG. (**C**) Cytidylyltransferase inhibition by HePC resulting in reduced phosphatidylcholine levels. (**D**) Reduced levels of IP_3 and DAG cause blockade of PI3K/AKT (cell survival) pathway and MAPK/ERK (cell proliferation) pathway. (**E**) HePC promotes SAPK/JNK (cell apoptotic pathway), which results in membrane disruption and cellular damage.

upregulation of the stress-activated protein kinase (SAPK)/c-Jun N-terminal kinase (JNK) pathway that mediates cellular stress and apoptotic signalling. Moreover, HePC significantly attenuates the mitogen-activated protein kinase (MAPK)/extracellular signal-regulated kinase (ERK) pathway that is responsible for cell proliferation, division, and growth. These events ultimately lead to tumour cell stress, membrane disruption, and apoptosis.[10] However, some limitations of HePC have reduced its use in cancer treatment, including hemolysis of erythrocytes and its rapid elimination from the bloodstream after intravenous (IV) administration.[11,12]

Recently, a number of lipid-based nano-delivery systems have been reported for targeted tumour delivery of anticancer agents, including solid lipid nanoparticles (SLNs),[3] nanoemulsions,[13] nanolipid carriers (NLCs),[14] nanoparticles,[6] and liposomes.[15] These nano formulations were used to administer drugs through various routes.[16] Moreover, they changed the basic physicochemical and biological properties of the drugs, and they improved drug release, targeting, and stability and reduced drug-related toxicities.[17–19] In order to address the abovementioned limitations of HePC in the present study, an NLC system was used. To the best of our knowledge, no NLC system has been reported to date for the delivery of HePC. NLCs are colloidal carrier systems comprised of both solid and liquid lipids and are categorised as second generation lipid nanoparticles. NLCs have been effectively used to increase loading capacity, prevent drug leakage, and provide increased modulation flexibility.[20,21] NLCs possess several advantages, such as enhanced targeting, drug safety, biodegradability, controlled release with reduced toxic effects of the loaded drugs, no requirement for organic solvents in their production, and high entrapment capability of both lipophilic and hydrophilic drugs.[22–24] Furthermore, NLCs improve drug solubility and penetration capacity and enhance the bioavailability and antitumor effects of the incorporated drugs.[14,25]

In the current study, we aimed to fabricate HePC-loaded NLCs possessing significantly reduced hemolytic potential and significantly enhanced antitumor efficacy. The HePC-NLCs were developed using a microemulsion technique that utilized a solid lipid, namely stearic acid, along with oleic acid as the liquid lipid. The hemolytic activity of the HePC-NLCs was determined, followed by an investigation of their cytotoxic effects on the MCF-7 and SCC-7 cell lines. Moreover, pharmacokinetic and antitumor analyses were performed to assess the bioavailability and anticancer potential of the HePC-NLCs, respectively. Our data suggest that an enhanced permeation and retention (EPR) effect facilitates the passive targeted delivery of the HePC-NLCs to tumour cells (Figure 2). Comprehensively, the neovasculature surrounding the tumour mass possesses a highly permeable vascular endothelium with large fenestrations of up to 4 μm.[26,27] Together with an impaired lymphatic clearance of the tumour microenvironment,[28] the atypical vascular endothelium promotes the accumulation of HePC-NLCs in the tumour surroundings. Enhanced buildup of HePC-NLCs in the tumour microenvironment would ultimately result in increased tumour cell internalisation and antitumor effects of the HePC entrapped within the NLCs.

Materials and Methods

Chemicals and Reagents

HePC was purchased from Shaanxi Yuantai Biological Technology Co., Ltd., China. Potassium dihydrogen phosphate and stearic acid were obtained from BDH (Laboratory Poole, England). Tween 80, oleic acid, sodium chloride, and sodium hydroxide were purchased from Sigma-Aldrich, Germany. Disodium hydrogen phosphate was purchased from Duksan (Ansan, Korea). Triton X-100 and rhodamine 6G chloride (R6G) were purchased from Merck (New York, USA). Dialysis tubing was purchased from Creative BioMart (New York, USA). The MCF-7, SCC-7, and 4T1 cell lines were purchased from the Korean Cell Bank (Seoul, South Korea). The cell lines were cultured in Dulbecco's modified Eagle's medium (DMEM) supplemented with 10% and 1% foetal bovine serum (FBS) and penicillin/streptomycin, respectively. Further, incubation at 37 °C was performed using a humidified CO_2 incubator. All other materials used in this study were of analytical grade.

Animals

For the in vivo evaluation, Sprague–Dawley rats weighing 250–280 g and female BALB/c mice weighing 18–20 g were obtained from Riphah International University, Islamabad, Pakistan. All animal procedures were approved by the Ethics Committee of Quaid-i-Azam University, Islamabad, Pakistan. All standard procedures for animals, before, during, and after experimentation, were carried out according to the guidelines set by the National Institutes of Health (NIH) for this purpose.

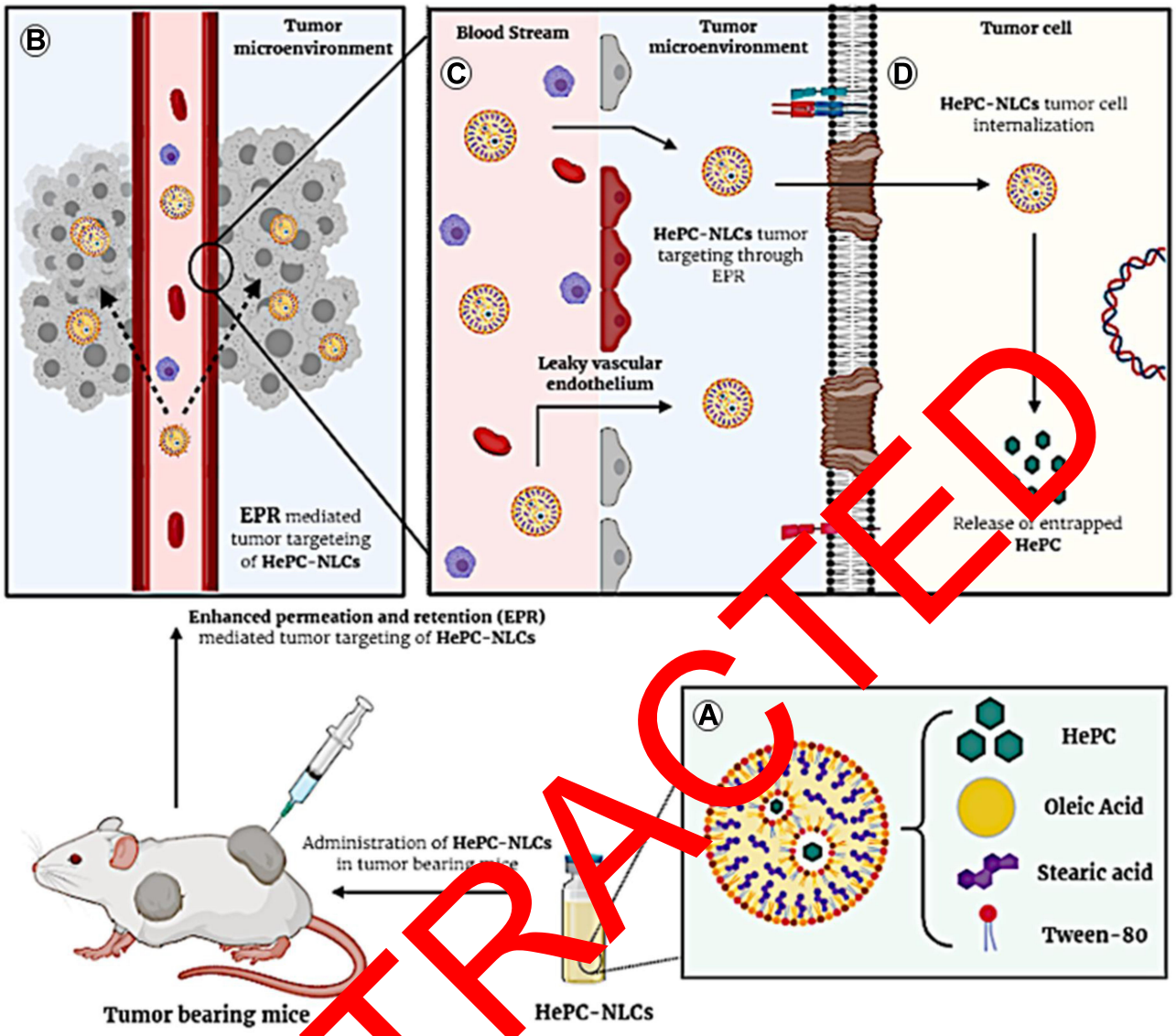

Figure 2 The representative diagram of tumor cell internalization via enhanced permeability effect (EPR) effect. (**A**) General structure of HePC-NLCs & its administration at tumor site. (**B**) EPR mediated passive targeting of HePC-NLCs. (**C**) Detailed description of the EPR effect via defectively fenestrated and leaky endothelium of tumor neovasculature. (**D**) Internalization of HePC-NLCs due to high membrane permeability of the tumor cells.

Preparation of HePC-NLCs

A modified microemulsion method was used for the preparation of HePC-NLCs. In order to obtain a clear and homogenous mixture, the oily phase solid lipid (stearic acid), liquid lipid (oleic acid), and drug (HePC) were heated to 80 °C, which is approximately 10–15 °C beyond the melting point of stearic acid. The surfactant (Tween 80) was dispersed in distilled water to prepare the aqueous phase, which was also heated using a magnetic stirrer at 80 °C. The aqueous phase was then gradually added to the melted oil phase with magnetic stirring at 750 rpm for 1 h, while the temperature was held at 80 °C. The resulting pre-emulsion was homogenised using a high-shear homogeniser at 9000 rpm for 15 min. Finally, one volume of microemulsion was dispersed in nine volumes of distilled water (chilled at 2–3 °C) to obtain the HePC-NLC dispersion.[29,30] The R6G-labelled NLCs were prepared using the same method, with the R6G added to the aqueous phase.

Characterisation of HePC-NLCs

Particle Size, Polydispersity Index (PDI), and Zeta Potential Analysis

The mean particle size, PDI, and zeta potential of the HePC-NLC dispersion were determined using a ZS 90

C zetasizer, furnished with a He-Ne laser operating at a wavelength of 635 nm. All measurements were carried out at a fixed light incidence angle of 90° and 25° using Zetasizer software, ver. 6.34 (Malvern Instruments Ltd, UK). Prior to the investigation, 10 µL of the HePC-NLC sample was diluted with 1 mL deionised water, followed by vortexing for 1 min.[31,32]

Incorporation Efficiency

The incorporation efficiency of HePC-NLCs was determined by measuring the concentration of the free drug in the supernatant. One millilitre of the formulation was centrifuged at 13,500 rpm for 1.5 h at 4 °C. The clear supernatant was diluted in distilled water at a ratio of 1:100 (50 µL supernatant in 5 mL distilled water). The free drug content of the supernatant was quantified using liquid chromatography-mass spectrometry (LC-MS).[33] The LC-MS apparatus consisted of an MS and ultra-high-performance liquid chromatography (UHPLC) system (Thermo Fischer Scientific, USA) connected to an electrospray ionisation source. The UHPLC system contained a BEH C18 column (1.7 µm bead size, 2.1×100 mm), an auto-sampler, and a binary pump. The system was operated at 40 °C and elution was carried out at 0.35 mL/min. The mobile phase was composed of 0.1% formic acid in water (A) and 0.1% formic acid in acetonitrile (B). Various ratios (A:B of 50:50 and 95:5 v/v) of the mobile phases were used to separate the drug. Initially, a 50:50 ratio was used for 2 min followed by changing to a 95:5 ratio for an extended period of 3 min. This ratio was maintained for 1 min, and then reset to 50:50. The collision gas pressure was maintained at 1.5 mTorr using *m/z* 405.4→125 with a collision energy of 29.1. The vaporiser temperature and spray voltage were maintained at 325 °C and 3.5 kV, respectively. Data analysis was performed using Thermo Xcalibur software. The incorporation efficiency was determined as

$$\%\text{incorporationefficiency} = \text{Wt} - \text{Wf}/\text{Wt} \times 100$$

where Wt is the total drug concentration and Wf is the concentration of free drug in the supernatant of the NLC dispersion.

Transmission Electron Microscopy (TEM)

The morphology of the HePC-NLCs was analysed using TEM (Hitachi H7600, Japan). The sample, in the form of a drop, was adsorbed onto a carbon-coated copper grid. The film on the grid was negatively stained by the addition of 2% (w/w) phosphotungstic acid solution. An accelerated voltage of 100 kV was used to observe the grid.[34,35]

Differential Scanning Calorimetry (DSC)

Thermal analysis of pure HePC, stearic acid, their physical mixture, and HePC-NLCs was accomplished using DSC (Q20, Delaware, USA). Briefly, a test sample (5 mg) was placed in an aluminium pan using an electronic weighing balance, and the pan was sealed with an aluminium lid. For reference purposes, an empty aluminium pan was used. The DSC temperature was uniformly increased from 20 °C to 300 °C at a rate of 10 °C/min. The flow of the nitrogen purge gas was maintained at 30 mL/min.[36]

X-Ray Diffraction (XRD)

XRD analysis was performed to analyse the crystallinity of the pure HePC, stearic acid, their physical mixture, and HePC-NLCs. For this purpose, Cu Kα radiations were used and the process was performed at 40 mA current and a constant voltage of 40 kV. Scanning was performed with a 2θ range from 10° to 80° with an increase of 5°/min.[37]

In vitro Drug Release Test

To explore the in vitro release behaviour of the HePC-NLCs compared with that of the pure drug, the dialysis bag method was employed. The process was performed at a pH of 7.4. Pure drug and HePC-NLCs equivalent to 10 mg of entrapped HePC were placed separately inside dialysis membrane tubing. Both ends were tied using thread to form a dialysis bag. The bags were then positioned inside a USP dissolution testing system (Vision Classic 6, LA, USA) filled with 500 mL of preheated dissolution medium. The apparatus was maintained at a constant shaking rate of 80 rpm and temperature of 36.5 °C ± 0.5 °C to mimic physiological conditions. At predesignated time periods, the dissolution medium (3 mL) was sampled for drug concentration analysis and replenished with an equal volume of fresh medium.[38] The collected samples were analysed using LC-MS, as described earlier.

In vitro Hemolytic Assay

The in vitro analysis of the inhibition of erythrocyte hemolysis was performed as reported by Wang et al.[39] Blood samples (10 mL) were obtained from healthy volunteers in prefilled K_2-EDTA tubes. The collected blood samples were centrifuged for 10 min at 1500 rpm to separate the

erythrocytes (RBCs). The RBCs were then washed three times with phosphate-buffered saline (PBS, pH 7.4) to eliminate serum proteins and debris. The transparent supernatant after each centrifugation was removed carefully and discarded. A 50% v/v suspension of RBCs was prepared in PBS and stored at 4 °C for ≤ 48 h. Fifty microliters of RBC suspension was added to PBS (950 µL) containing different concentrations of HePC-NLCs or HePC alone, for the purpose of assessing hemolysis. Triton X-100 (1% v/v in water) and PBS were used as the positive control (100% lysis) and negative control (0% lysis), respectively. All samples were then incubated in an Eppendorf thermomixer for 1 h. The mixing frequency and temperature were adjusted to 450 rpm and 37 °C, respectively. Intact erythrocytes were isolated by centrifugation at 10,000 rpm for 5 min. Finally, the absorbance at 540 nm of the supernatant was measured. The following equation was used to determine the percent hemolysis:

$$\%\text{hemolysis} = \frac{A_{\text{sample}} - A_{\text{negativecontrol}}}{A_{\text{positivecontrol}} - A_{\text{negativecontrol}}} \times 100$$

In vitro Cytotoxicity Studies

An in vitro cytotoxicity study of HePC and HePC-NLCs was carried out using the MTT (3-(4,5-dimethylthiazol-2-yl)-2,5-diphenyltetrazolium bromide) colorimetric assay. The assay was performed in 96-well plates by seeding previously isolated cells at a concentration of cells/mL. The cells were incubated at 36.5 °C in a 5% CO_2 atmosphere for 24 h. Then, the cells were treated with various concentrations (0.1, 0.25, 0.5, 1.0, 2.5, 5.0, 12.5, 25.0, 50.0, and 75.0 µg/mL) of blank NLCs, HePC-NLCs, or HePC under the same incubation conditions for 24 h. Afterwards, 20 µL of MTT solution was added to each well and incubated for another 4 h. Finally, 100 µL of dimethyl sulfoxide (DMSO) was added to each well to dissolve the formazan crystals that were produced. The absorbance at 595 nm of each well was measured using a microplate reader.[40]

The percentage of viable cells (% viability) was calculated using the following equation:

$$\%\text{Viability} = \frac{AT - AB}{AC - AB} \times 100$$

where AT is the A_{595} of the treated sample, AB is the A_{595} of the blank, and AC is the A_{595} of the control. The percent cytotoxicity (% cytotoxicity) was also obtained by subtracting the % viability from 100.

Cellular Uptake Study

An extensively employed fluorescent dye to assess the cellular uptake of hydrophilic drugs,[41] R6G, was utilised to track the uptake of NLCs by tumour cells. MCF-7 cells at a density of 5×10^4 cells/well were placed into 6-well plates and incubated for 24 h. The cells were then exposed to medium containing R6G (12.5 µg/mL)-labelled HePC-NLCs for another 24 h. The cells were then washed with cold PBS and fixed with 70% ethanol for 30 min. Afterward, the cells were washed with PBS and stained with DAPI (4′,6-diamidino-2-phenylindole) for 15 min to visualise their nuclei. Finally, the cells were washed with PBS to remove excess DAPI and observed under a fluorescence microscope (Olympus IX71 microscope, Japan).[42]

Pharmacokinetics Study

A pharmacokinetic study of the HePC formulations was performed in male Sprague–Dawley rats. The rats were divided into two groups with six rats per group. One group was administered HePC-NLCs (5 mg/kg, IV), and the other group was administered an equivalent amount of pure drug. The rats were housed in an animal house according to the approved guidelines of Quaid-i-Azam University, Islamabad and the NIH. The room temperature was maintained, and the humidity was set to 50–60% relative humidity. Prior to the experiment, the rats were fasted for 12 h. Blood samples (0.3 mL) were collected from the femoral artery in heparinized Eppendorf tubes at pre-specified time intervals. The plasma was separated from the blood samples through centrifugation, which was stored at −20 °C for further use.[19,43,44]

Plasma Sample Processing

Blood plasma (150 µL) was mixed with acetonitrile (150 µL). The mixture was vortexed and centrifuged, and 20 µL of the supernatant was analysed using LC-MS to determine the quantity of the entrapped HePC, as described earlier.

Biodistribution and Toxicity Studies

To carry out these studies, 12 Sprague–Dawley rats were segregated into two groups; one group was administered a single IV dose of pure drug (5 mg/kg) and the other group was administered an equivalent dose of HePC-NLCs. Three rats from both groups were euthanised after 1 h, and the remaining rats were euthanised after 12 h. The

organs of the euthanised rats (liver, kidneys, lungs, heart, and spleen) were isolated, washed twice with cold normal saline, dried at room temperature, and stored at −20 °C prior to analysis.[45] To quantify HePC concentrations in the organs, the tissues (0.5 g) were homogenised in 3 mL PBS, clarified by centrifugation at 20,000 rpm for 5 min, and subjected to LC-MS, as described earlier. All experiments were conducted according to approved ethical considerations and guidelines for animal studies. In addition, liver toxicity in the HePC-NLC-treated rats was assessed by haematoxylin and eosin (H&E) staining to visualise any injury or inflammation.

Breast Tumour Formation in Mice

4T1 cells (2×10^6) were mixed with Matrigel (200 µL) and injected into the fourth mammary fat pad of 6-week-old female BALB/c mice. The mice were then divided into three groups (one control and two experimental groups), with each group comprised of nine mice. Normal saline was administered to the control group. The other two groups received pure drug or HePC-NLCs at a dose of 5 mg/kg on days 3, 6, 9, and 12. The animals were observed twice daily for clinical abnormalities. Body weight changes were assessed to evaluate the tumour weight and toxicity of each formulation. The body weights of individual mice were obtained prior to dosing on day 1 and after dosing on days 3, 6, 9, 12, 15, 19, and 21. The mice were also checked for survival daily, and the mean survival time (MST) and percentage of increased life span (ILS) were determined. Finally, the length and width of each tumour were measured using callipers, and tumour volume was calculated as follows: V = (length × width^2)/2.[4,19]

Immunohistochemistry Study

Immunohistochemical experiments were conducted using primary immunoglobulins in combination with the avidin-biotin peroxidase complex (ABC) and peroxidase substrate kit (Vector Laboratories Inc., Burlingame, USA) to evaluate the levels of the tumour-expressed apoptotic markers, poly (ADP-ribose) polymerase (PARP) and caspase-3.[46] Initially, the tumour sections were subjected to heat-based epitope retrieval (95–100 °C) using citrate buffer (10 mM) with a pH of 6.0.[47] Afterward, endogenous tumour peroxidase activity was inhibited by incubating the sections for 30 min in a methanolic solution of 0.3% H_2O_2. Non-specific antibody binding was then blocked by incubating the sections in horse serum blocking solution in a temperature-humidity chamber for 1 h. The sections were then incubated with primary antisera at 4 °C overnight. Subsequently, the sections were incubated for 1 h at 25 °C with biotinylated universal secondary antibody and ABC. Finally, the tumour sections were incubated with peroxidase substrate at room temperature for 3 min. After every step, all of the sections were rinsed three times with 0.01 M PBS. All cells displaying cytoplasmic immunoreactivities above 20% of the background density for individual apoptotic markers were considered positive. The immunoreactivity region (%/mm^2 of tumour mass), the region of tumour mass dominated by PARP and caspase-3 expression, was assessed using an automated image analyser.[48]

TUNEL Assay

The TUNEL assay is usually used to detect DNA fragmentation that occurs during apoptosis. In this study, the TUNEL assay (Roche Applied Science, Indianapolis, IN) was performed to confirm apoptosis in tumour tissues. Briefly, the tumour sections were fixed with 4% paraformaldehyde, followed by deparaffinization using xylene and alcohol. The sections were stained, and TUNEL-positive nuclei were observed using a fluorescence microscope.[50]

Statistical Analysis

Numerous statistical assessment tests were conducted to compare the test groups in this study. Variance homogeneity was assessed using Levene's test. When no meaningful differences were obtained in variance, one-way ANOVA was used, followed by the least-significant differences (LSD) multi-comparison test to check for significant differences. In case of a meaningful change in variance, the data were further analysed with the Kruskal–Wallis *H*-test. Statistical analyses were performed using SPSS for Windows (Release 22.0K, SPSS Inc., Chicago, IL, USA). Data were acquired in triplicate or sextuplicate and were significantly different if the p value was < 0.05. Sigma plot (version 12.5) was used to plot the graphs. To understand antitumor potential, % point changes among vehicle-control tumour masses and test material-treated tumour masses were estimated by utilising the following equation.

$$\text{Percent point changes compared with vehicle control}(\%) = \left(\begin{pmatrix} \text{Data of test material} - \text{treated masses} \\ -\text{Data of vehicle} - \text{control masses} \end{pmatrix} / \text{Data of vehicle} - \text{control masses} \right) \times 100$$

Results and Discussion

NLCs are prepared by various methods, but the microemulsion method is one of the most convenient owing to its ease of production, better yields, and controlled release of the formulation.[51] The main components of NLCs are lipids (solid and liquid), water, and emulsifiers. Generally, the ratio of solid to liquid lipids ranges from 70:30 to 99:1, whereas the surfactant concentration ranges from 1.5% to 5% (w/v).[52] Commonly used solid lipids for NLC preparation include Compritol® 888 ATO, Precirol® ATO5, fatty acids, triglycerides, steroids, and waxes. The liquid oils used in NLCs are mostly digestible oils from natural sources. Medium chain triglycerides (Miglyol® 812), paraffin oil, 2-octyl dodecanol, isopropyl myristate, and squalene have been used as liquid lipids. Fatty acids, such as oleic acid, linoleic acid, and decanoic acid, may also be used as liquid lipids.[23]

Preparation of HePC-Loaded NLCs

In a recent study, the microemulsion technique was used to prepare HePC-NLCs because of the formation of uniformly sized particles and stability of the formulation over an extended period of time.[41] Previously, fluticasone propionate, transferrin-decorated paclitaxel, and curcumin-loaded NLCs have been successfully prepared by this method.[53–55] In the present study, the NLCs comprised two types of lipids, solid and liquid lipids, and a drug. A surfactant was also employed to stabilise the designed NLCs. The final composition of the selected formulation was stearic acid/oleic acid/Tween 80/HePC/distilled water (6/4/1/0.75/10, w/v). Stearic acid and oleic acid were selected because of their high drug solubility. Similarly, based on its appropriate hydrophilic-lipophilic balance (HLB) value, Tween 80 was included as a surfactant. It is usually suggested to select lipids and surfactants within a narrow range of HLB values for the preparation of oil-in-water (o/w) emulsions.[56] Because the HLB values of both components lie between 14 and 15, they were selected for preparation of the NLCs. The NLCs were then characterised in terms of their particle size, PDI, zeta potential, and incorporation efficiency.[20]

Characterisation of HePC-Loaded NLCs

Particle Size, PDI, and Zeta Potential

Using dynamic light scattering analysis, the mean particle size and PDI of the HePC-NLCs were respectively obtained as 143.8 ± 16.2 nm and 0.104 ± 0.002, signifying that the formulation was nanosized and monodispersed (Figure 3A). Zeta potential analysis using the Zetasizer ZS90 revealed a negative charge (−34.2 ± 1.2 mV) on the particle surfaces (Figure 3B), indicating the stability of the formulation. The formation of nanoparticles with uniform distribution and stability usually depends on the process parameters and method of preparation. As discussed earlier, the microemulsion technique produces NLCs with suitable characteristics for drug delivery.[23]

Incorporation Efficiency

The incorporation efficiency of the HePC-NLCs was 91.13 ± 7.2%. This enhanced incorporation efficiency can be attributed to the NLC matrix containing stearic acid. The addition of oleic acid, as a co-lipid, with the solid lipid produces more space for drug incorporation. Moreover, the addition of oleic acid increases drug solubility in the NLC matrix, leading to enhanced drug incorporation.[57]

Transmission Electron Microscopy

TEM was used to evaluate the morphological features of the HePC-NLCs. The particles were found to be spherical with clear boundaries and sizes less than 200 nm. Additionally, the results demonstrated the monodispersibility of the HePC-NLCs, as shown in Figure 3C.

Thermal Analysis

The thermal analyses of pure HePC, stearic acid, their physical mixture, and HePC-NLCs are shown in Figure 4A. The physical mixture was prepared by combining HePC and stearic acid without any other additives. As shown in Figure 4A, clear endothermic peaks at 40 °C, 100 °C, and 246 °C are visible with pure HePC, which are probably due to the loss of moisture content, loss of hydrated water, and melting of the HePC, respectively, followed by decomposition of the drug. Stearic acid displayed a slight endothermic profile at 56 °C. In addition, the physical mixture exhibited a relatively low intensity of the HePC and stearic acid peaks at their corresponding positions. In contrast, the HePC and stearic acid peaks are not evident in the thermal analysis of the HePC-NLCs, demonstrating transformation of the drug into an amorphous form when incorporated into the NLCs.

PXRD Analysis

Figure 4B shows the PXRD analysis of pure HePC, stearic acid, their physical mixture, and the HePC-NLCs. The X-ray diffractogram of pure HePC showed characteristic

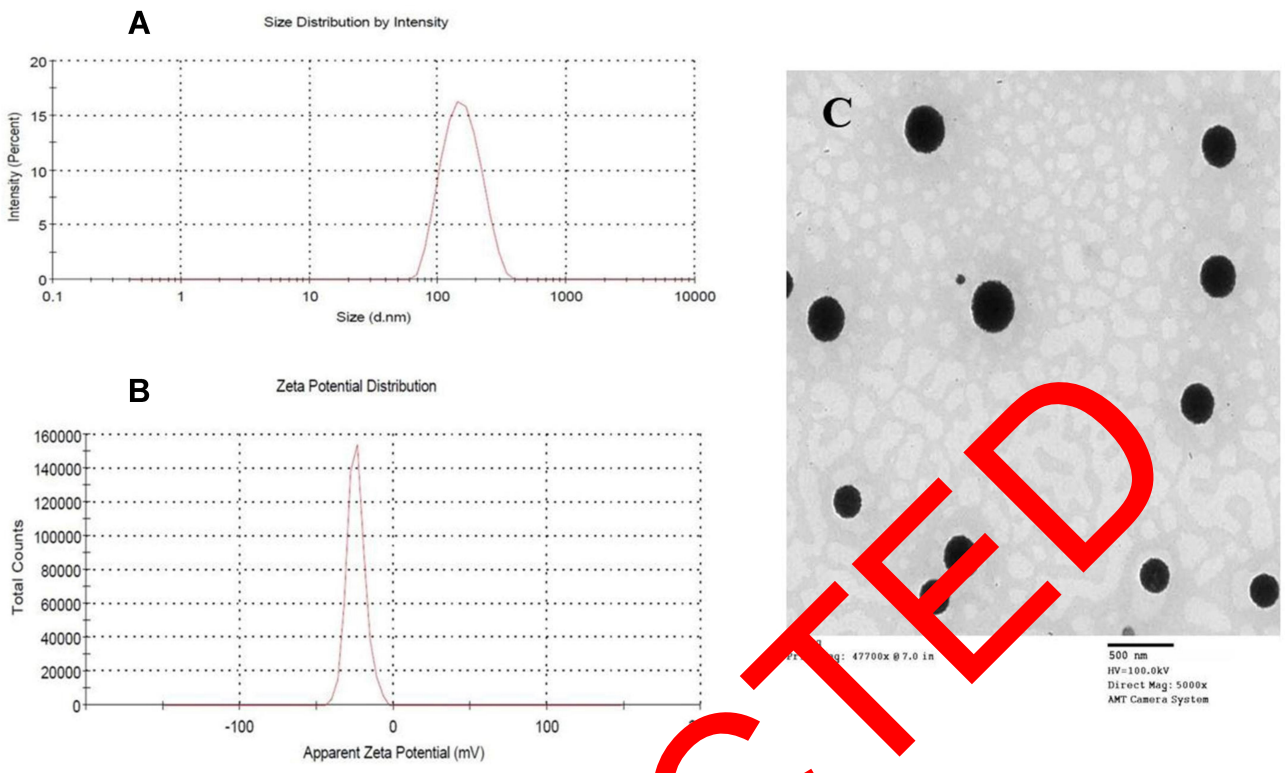

Figure 3 Characterisation of HePC-NLCs: (**A**) Average hydrodynamic particle size of HePC-NLCs; (**B**) Zeta potential distribution of HePC-NLCs; (**C**) TEM-mediated morphology analysis of HePC-NLCs (10,000×).

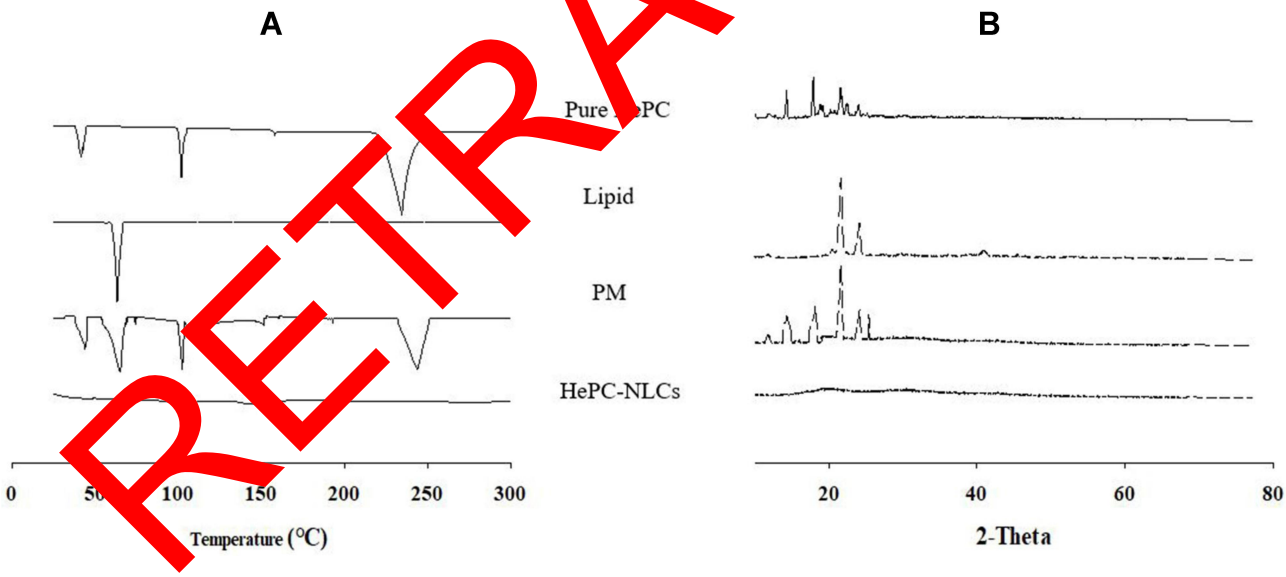

Figure 4 Solid-state characterization of HePC-NLCs, pure HePC, lipid, and lipid mixture: (**A**) Dynamic scanning calorimetry (DSC) analysis; (**B**) Powder X-ray diffraction (PXRD) analysis.

crystalline peaks at 2θ of 11.8°, 14.3°, 17.8°, 18.7°, 21.4°, 22.3°, and 24°. Similarly, stearic acid showed crystalline peaks at 21.6° and 22.4°. The physical mixture produced all the characteristic peaks of pure HePC and stearic acid, demonstrating that HePC exists in a crystalline form when simply mixed with stearic acid. However, the corresponding peaks were absent in the HePC-NLC diffractogram, indicating transformation of the drug from a crystalline to amorphous state. This analysis demonstrated the successful incorporation of HePC into NLCs.

In vitro Drug Release

The in vitro release of HePC from the HePC-NLCs was evaluated at pH 7.4, and was compared with a pure drug solution. The medium was maintained at 37 °C. Burst release was observed from the pure drug solution, as the majority of the drug was released in the first 30 min, followed by complete release within 4 h. Only 16% of the drug was released from the HePC-NLCs after 30 min, followed by 51% release by 24 h (Figure 5A). In contrast to the pure HePC solution, the HePC-NLCs clearly exhibited sustained drug release behaviour. The burst release of HePC from the solution could be attributed to the hydrophilic nature of the drug. Moreover, the drug entrapment in the lipid milieu of NLCs has been shown previously to produce a sustained and slow release of the drug.[58,59] Thus, enhanced HePC entrapment, reduced HePC loss during storage, and controlled release of HePC were attained with the HePC-NLC formulation. Another reason for the high drug payload is the overall increase in the solid lipid component of the NLCs.[60] Additionally, one of the major problems previously noted with this drug was its quick release from the body upon IV administration. Our in vi[illegible] release data demonstrated extended discharge of th[illegible] drug from the HePC-NLCs. However, pharmacokinetic [illegible] studies are required to confirm these result[illegible] in vi[illegible].

In vitro Hemolysis

Figure 5B and Table 1 show the percent comparative hemolysis at various concentrations of the pure drug and HePC-NLCs. The pure drug showed 93% hemolytic activity even at a low concentration of 3.125 µg/mL, whereas at higher concentrations, 100% hemolytic activity was observed. Unlike pure HePC, less than 8% hemolytic activity occurred with the HePC-NLCs for all tested concentrations. Thus, the HePC-NLCs demonstrated significantly reduced hemolytic activity compared to that of the pure drug.[7] This reduced hemolytic activity may be attributed t[illegible] protective effect and controlled release profile of th[illegible]LCs when[illegible]sed for the loading of HePC. Moreover, a red[illegible]tion in the [illegible]emolytic potential of HePC has bee[illegible] reported [illegible] other [illegible]arrier systems such as liposomes[illegible]nd albu[illegible]n micr[illegible]rticles.[61,62]

In vitro Cy[illegible]toxicity

The cytotox[illegible]ity pr[illegible]les of the test formulations, including pure dr[illegible]blank NLCs[illegible]nd HePC-NLCs, were evaluated to d[illegible]ermine their efficacy against cancer cells, as shown in [illegible]gure 6A a[illegible] B. The blank NLCs did not display cyto[illegible]icity at a[illegible] drug concentration; more than 90% of the cells, [illegible]dless of the cell line, remained viable even aft[illegible]4 h of contact with the formulation, indicating its [illegible]iocompatible nature and tolerability.[40,63] The pure drug [illegible]emonstrated significantly enhanced cytotoxicity and

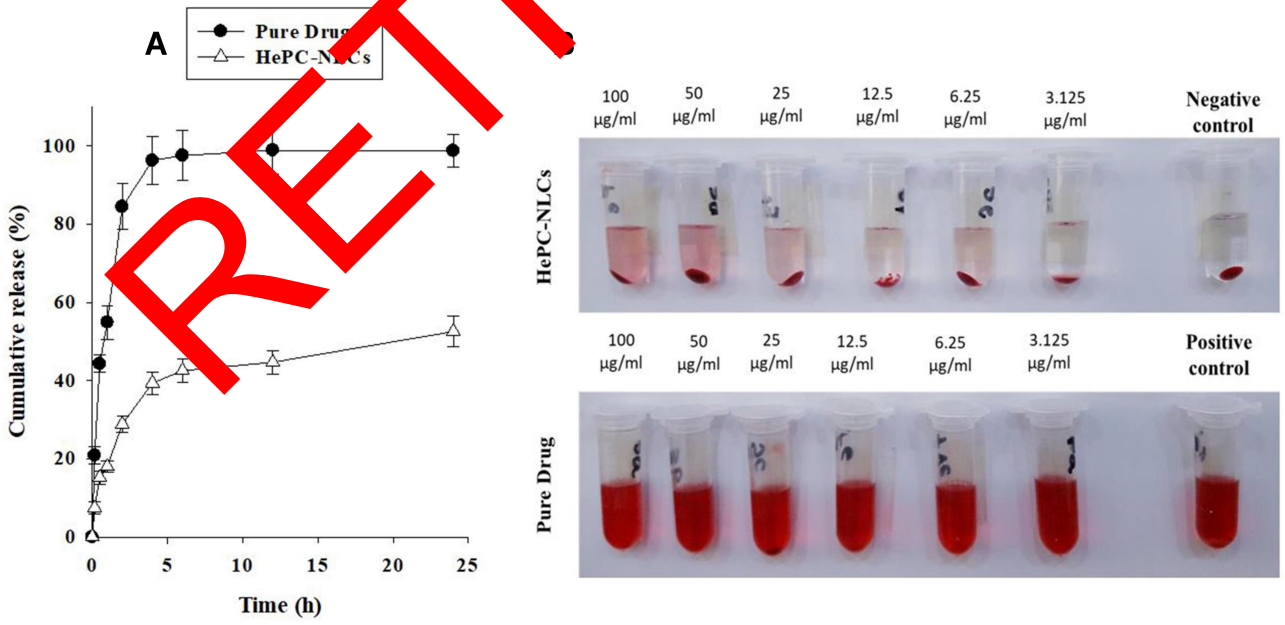

Figure 5 In vitro cumulative release (**A**) and % hemolysis vs drug concentration data (**B**), of the HePC-NLCs compared with that of the pure drug (HePC). Numbers 1–6 in % hemolysis represent 3.125 µg/mL, 6.25 µg/ mL, 12.5 µg/ mL, 25 µg/ mL, 50 µg/ mL, and 100 µg/ mL, respectively. Each value represents the mean ± S.D. (n = 3).

Table 1 In vitro Haemolytic Activity of HePC-NLCs and HePC Solution at Various Drug Concentration

Drug Concentration (μg/mL)	HePC-NLCs	Pure Drug
3.125	90.49 ± 3.05*	1.06 ± 0.18
6.25	90.77 ± 3.78*	2.42 ± 0.32
12.5	91.78 ± 4.72*	2.74 ± 1.57
25	93.32 ± 4.90*	6.61 ± 1.52
50	96.34 ± 5.13*	6.75 ± 1.31
100	98.25 ± 4.21*	7.34 ±1.05

Notes: Data are expressed as mean ± S.D. (n=3). *$p < 0.05$ versus pure drug. Pure drug represent the HePC solution at equivalent drug concentration.

considerably reduced cell viability compared to that of the blank NLCs. This could be attributed to the cytotoxic effects of HePC. However, since HePC is quickly cleared from the bloodstream when administered in pure form, as demonstrated in pharmacokinetic studies, its cytotoxic effect does not persist. The HePC-NLCs significantly reduced the cell viability, as almost all the cancer cells died after treatment when compared to those of the blank NLCs and pure drug. Moreover, this result showed that the oil phase used in the preparation of NLCs may affect the cell viability. As reported earlier, drug-loaded NLCs, predominantly in preparation with oleic acid, could meaningfully reduce the viability of MCF 7 cells.[63] Furthermore, the improved activity of NLCs associated HePC may be correlated to the mode of entry of HePC-loaded NLCs into the cell. In its pure form, the drug is quickly eliminated from the body as demonstrated in the pharmacokinetic study; thus, the antitumor potential of the pure drug is short-lived. However, upon incorporation into the NLC system, the drug was observed to stay in bloodstream for an extended period of time, emphasising the improved apoptotic effect of the HePC-NLCs.[4,17,20,45,48] Furthermore, the IC$_{50}$ values of the pure drug and HePC-NLCs were respectively found to be 38.21 ± 0.85 μg/mL and 10.2 ± 0.12 μg/mL for MCF 7 cells and 51.67 ± 0.93 μg/mL and 18.1 ± 0.5 μg/mL for SSC 7 cells (Table 1). These results demonstrated the enhanced activity of the HePC-NLCs in both the tumor cells.

Cellular Uptake Study

The cellular uptake study was performed by fluorescence imaging of MFC-7 cells after incubating with R6G-labelled HePC-NLCs. As shown in Figure 6C, the R6G-labelled HePC-NLCs were found alongside the cell nuclei after 24 h, indicating the cytoplasmic localization of the R6G-labelled HePC-NLCs. Thus, it can be concluded that the HePC-NLCs can be taken up by and internalised in the tumour cells to efficiently deliver the antitumor drug, resulting in a targeting effect that leads to enhanced antitumor efficacy. Tumour cell targeting is a prerequisite to ensure the therapeutic efficacy of a novel drug delivery system. In this regard, cell uptake studies are one of the most important studies designed to assess the cell and tumour internalisation of nanocarriers loaded with anticancer agents. Small drug molecules are incorporated into nanocarriers that can infiltrate tumour cells by either the EPR effect or through endocytosis to exhibit their cytotoxic effects (Figure 2).

Pharmacokinetic Parameters

Figure 7A shows the mean plasma concentration vs time curves of HePC after IV administration of the pure drug and HePC-NLCs. The mean plasma concentrations of HePC after IV injection of the HePC-NLCs were higher than those of the pure drug. As expected, the pure drug exhibited linear pharmacokinetics, as it was readily eliminated from systemic circulation,–4–5 h post-IV administration.[4,64] Half of the HePC was eliminated after 1.20 ± 0.26 h ($t_{1/2}$), with a reduced mean residence time of 0.7 ± 0.14 h, as compared to the HePC-NLCs, which exhibited values of 21.11 ± 0.72 h and 6.24 ± 0.93 h, respectively (Table 2). These results demonstrated that the drug level in the blood persisted for extended durations with HePC-NLC administration, resulting in enhanced therapeutic efficacy of the drug. Similarly, the area under the concentration time-curve from time zero to infinity ($AUC_{0-\infty}$) was significantly higher ($p < 0.05$) with the HePC-NLCs than with the pure drug. The significantly higher AUC and reduced elimination rate of the HePC-NLCs could be attributed to the steric stabilisation effect of stearic acid[56] in the NLCs, which provides protection from opsonisation, a vital property in drug delivery.[65] These findings demonstrate that HePC-NLCs can improve the efficacy of the incorporated drug, which may result in dose reductions.

Biodistribution and Toxicity Studies

In the highly perfused organs of rats, namely the heart, spleen, liver, kidneys, and lungs, the HePC concentration per tissue weight was quantified at 1 h and 12 h following a single IV dose of pure HePC and HePC-NLCs. The findings are shown in Figure 7B. The HePC concentration in the spleen and liver with the HePC-NLCs was significantly enhanced, in contrast to that with pure HePC. This

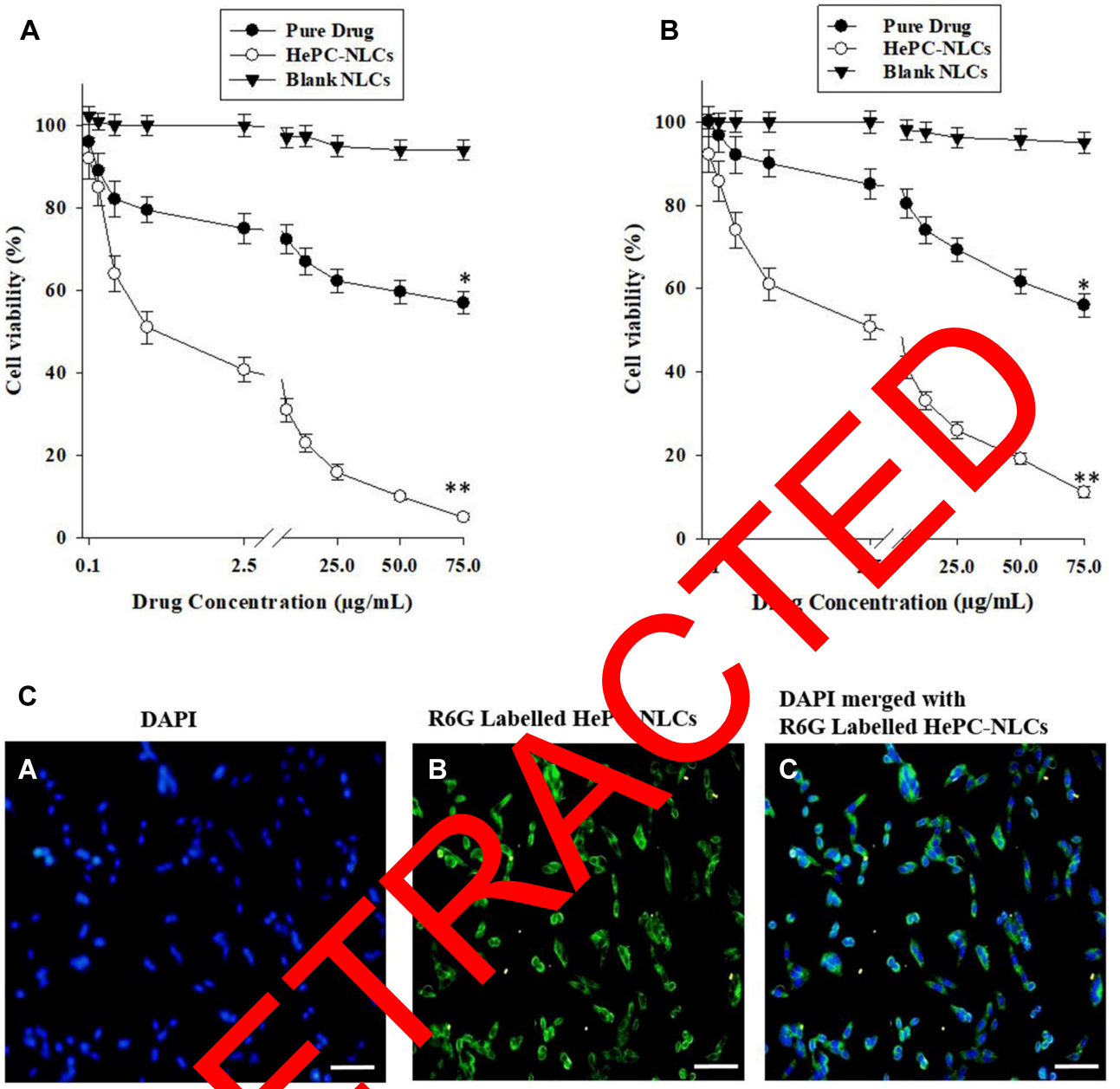

Figure 6 Cell viability ... concentration profile ... of HePC-NLCs, pure drug, and blank NLCs: (**A**) MFC-7 cells; (**B**) SCC-7 cells. Each value represents the mean ± S.D. (n = 3); (**C**) Fluorescence microscopic images ... C-7 cells treated with R6G-labelled HePC-NLCs. DAPI-stained cell nuclei, green fluorescence distributed in the cytoplasm of R6G-labelled ...Cs, and merged images ... shown. *Represents p<0.05 when compared with Blank NLCs and ** represents p<0.01 when compared with Blank NLCs and Pure Drug.

Abbreviations: DA... ...-diamidino-2-phenylindole; R6G, rhodamine 6G; HePC-NLCs, Miltefosine-loaded nano lipid carriers.

was probably due to enhanced drug release and biodistribution associated with the HePC-NLCs, which the pure HePC lacks. The drug concentration in other organs (heart, lungs, and kidneys) was extremely low and was not significantly different between the two HePC forms. The HePC concentration in various organs (heart, kidneys, lungs, and spleen) was also determined at 12 h. The results clearly demonstrated an equally low drug level compared with that at 1 h, owing to the minimised drug dissemination in normal body tissues and organs along with an improved drug safety profile. However, even at 12 h, a comparatively large concentration of HePC could be seen passing through the liver, indicating the sustained drug release that could be attributed to the long-lasting effect of the NLCs. Furthermore, this most likely was due to the long half-life of HePC. To exclude the possibility of

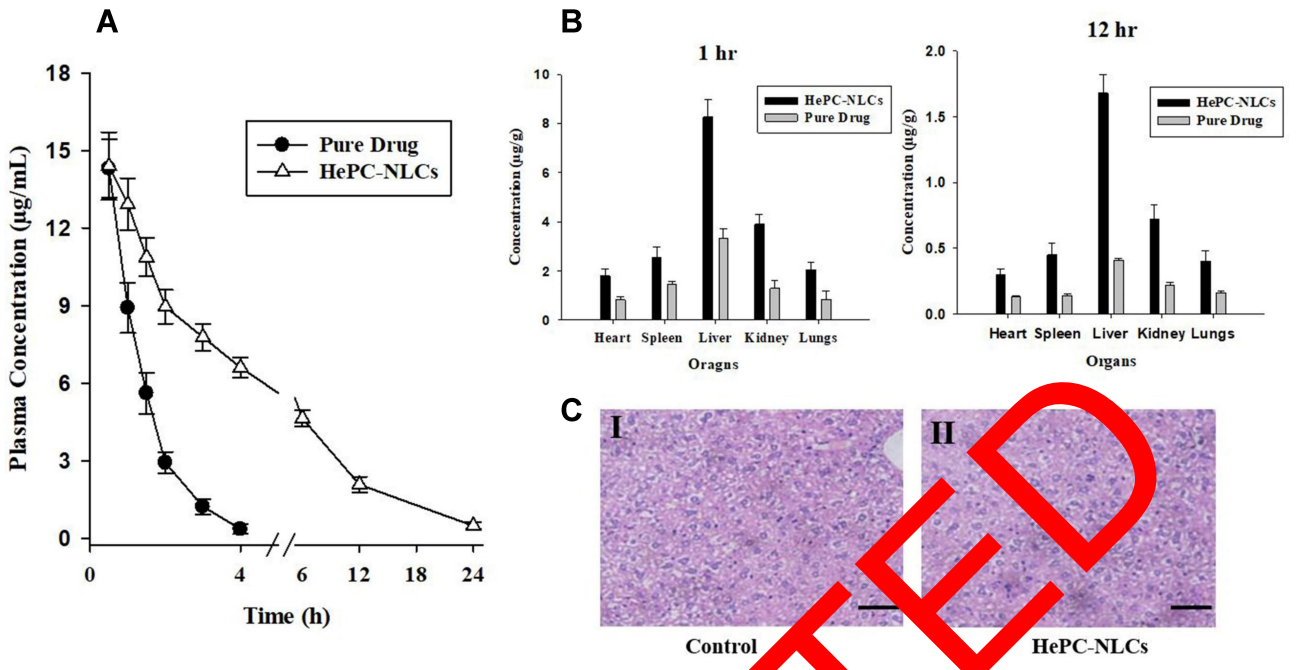

Figure 7 (**A**) Plasma concentration-time profiles of HePC after intravenous administration of HePC-NLCs and pure drug in rats. Each value represents the mean ± S.D. (n = 6). All values for HePC-NLCs at each time were significantly different from those for pure drug, $p < 0.05$; (**B**) Heart accumulation in major organs of the rats 1 h and 12 h after administration of HePC-NLCs and pure drug. Data are given as means ± S.D. (n = 6); (**C**) Representative H&E stained segments of hepatic tissue of mice at 200× magnification to determine hepatotoxicity, (I) normal histological structure of the hepatic lobule, control (untreated liver) and (II) liver tissues treated with the HePC-NLCs.

liver toxicity, an additional study of liver pathology after HePC-NLC administration was conducted, and the results were compared with those of the control (Figure 7C). H&E staining of the liver tissue demonstrated no significant alterations, inflammation, injury, or signs of irritation in the liver tissues. Thus, it can be concluded that the HePC-NLCs do not cause any overt sign of hepatic inflammation or toxicity.

Antitumour Study

The antitumour efficacy of the HePC-NLCs was assessed in BALB/c mice based on tumour volume and body weight changes and compared with the pure drug and normal saline (Figure 8A–C and Table 3).[48,66] After induction of the tumour, its size was constantly measured and treatment was started when the tumour reached 150–180 mm^3. The first dose was administered on day 3. The tumour volumes and body weights were significantly increased in the mice administered normal saline. This likely occurred because no antitumor drug treatment was administered. The pure drug-treated group showed significantly reduced tumour volumes and body weights compared to those of the normal saline group; however, these values were significantly higher than those of the HePC-NLC group. This could be attributed to the nonencapsulated drug's rapid elimination from the blood circulation, as demonstrated in pharmacokinetic studies.[67,68] Nevertheless, the HePC-NLCs demonstrated significantly reduced tumour volumes and sustained body weights compared to the values with pure drug and normal saline. This might be caused by its sustained release behaviour and longer retention in the bloodstream, as demonstrated by our in vitro release and in vivo pharmacokinetic studies. This experiment establishes the antitumor efficacy of NLCs when loaded with HePC. An important aspect of this study was the selection of an optimal dosing schedule for HePC, since it is rarely used for tumour targeting, and much remains to be discovered regarding its antitumor efficacy. Thus, an optimal dosage schedule (5 mg/kg; days 3, 6, 9, and 12) was adopted from a number of studies

Table 2 Pharmacokinetic Parameters of HePC After IV Administration of HePC-NLCs and Pure Drug (Equivalent to 5 mg/kg of HePC) to Rats

Parameters	HePC-NLCs	Pure Drug
$AUC_{0\to\infty}$ (μg·h/mL)	79.45 ± 9.93*	18.57 ± 1.26*
C_{max} (μg/mL)	14.40 ± 1.30	14.30 ± 1.13
$t_{1/2}$ (h)	21.11 ± 0.72*	13.2 ± 0.26
MRT (h)	6.24 ± 0.93*	0.78 ± 0.14

Notes: Data are expressed as mean ± S.D. (n=6). *$p < 0.05$ versus pure drug. Pure drug represent the HePC solution at equivalent drug concentration.

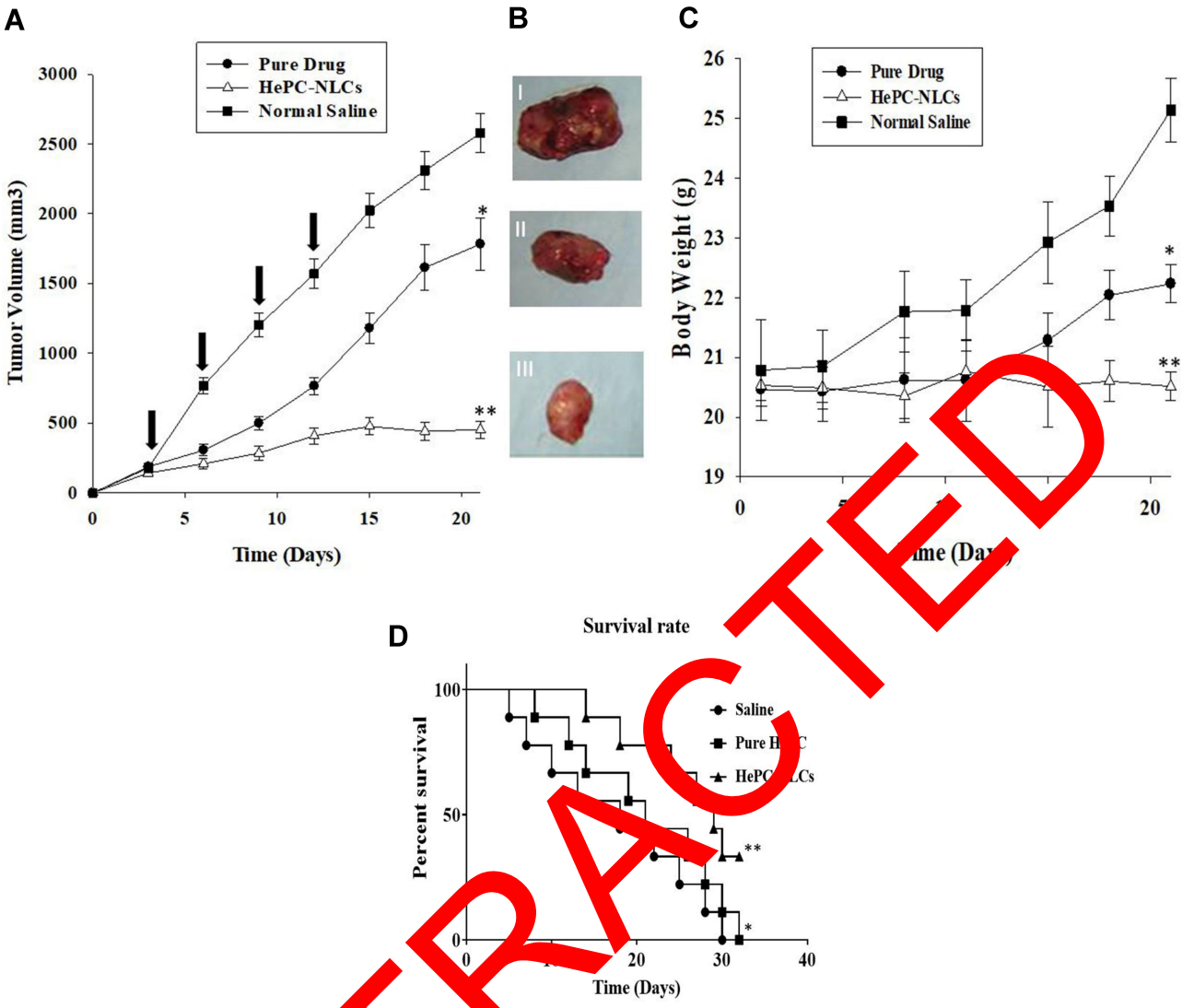

Figure 8 Antitumour efficacy after intravenous administration of HePC-NLCs, pure drug, and normal saline: (**A**) tumour volume analysis; (**B**) representative tumour mass after respective treatments; I, II, and III represent normal saline-, HePC solution-, and HePC-NLCs-treated groups, respectively; (**C**) body weight change. Arrows indicate the administration time points for HePC-NLCs, pure drug, and normal saline. Each value represents the mean ± S.D. (n = 6); (**D**) Effect of pure HePC and HePC-NLCs on the survival rate of BALB/c mice compared to that of the normal saline (untreated) (n = 9). *Represents p<0.05 when compared with Normal Saline and ** represents p<0.01 when compared with Normal Saline and Pure Drug.

recently reported various anticancer drugs,[4,17,42,45] in order to obtain efficacy signals which otherwise would need to be tested in advanced disease settings or in Phase I trials. An important strategy in this regard was the pharmacokinetic data, which revealed that administration of the HePC-NLCs at 5 mg/kg produced a C_{max} of 14.47 ± 0.4 and a C_{min} of 0.48 ± 0.13. Additionally, the overall drug content in the bloodstream over time (AUC) was sufficient to induce an antitumor effect. However, further studies on the use of different HePC dosing schedules need to be conducted.

Table 3 Therapeutic Efficacy of Various Formulations of HePC in BALB/c Mice Inoculated with 4T1 Cells

Treatment Groups	MST ± SD (Days)	Median (Days)	ILS (%)
Pure Drug	35.75 ± 3.93*	34*	9.83*
HePC-NLCs	42.19 ± 3.82**	41**	30.21**
Normal Saline	31.68 ± 3.59	29	——

Notes: Each value represents the mean ± SD (n=9). MST and ILS respectively stands for mean survival time and increased life span. *p <0.01 as compared with normal saline treated groups. **p <0.001 as compared with pure drug and normal saline treated groups.

Survival Rate Analysis

The survival rate of the tumour-bearing mice was also determined in response to the treatments administered to

eliminate the tumour. Figure 8D shows the survival rate as a Kaplan-Meier plot, whereas the MST and ILS values are tabulated in Table 3. The saline-treated mice could not survive due to tumour toxicity; the first mouse died on day 5, followed by consistent mortality until day 30, when all the mice had died due to presence of the tumour. Similarly, the first mouse died on day 9 after treatment with the pure drug. Unlike the saline-treated group, the survival rate of the mice was extended over many days with pure drug treatment; however, all the mice had died by day 32. In contrast, a significantly enhanced survival rate was observed in the HePC-NLC-treated mice. The first mouse died on day 15 and approximately 66% of the mice were still alive on day 32. The HePC-NLCs prolonged the survival rate of the mice significantly more than HePC alone or saline did. Despite the pure drug being less effective than the HePC-NLCs, it meaningfully improved survival rate of the mice as to that of normal saline. This study demonstrates the increased survival potential of HePC when incorporated into NLCs.

Histomorphometric Analysis

The outcomes of the histomorphometric analysis are provided in Table 4 and Figure 9A–C. Decreased tumour cell volumes and elevated caspase 3 and PARP immunopositive cells were documented following treatment, in the order of HePC-NLCs > pure drug >> saline. In particular, the HePC-NLC-treated tumours showed a significant ($p<0.01$) decrease in volume and a significant increase in the number of caspase-3 and PARP immunopositive cells compared with that of the pure drug- and saline-treated tumours. Apoptosis can be induced by mitochondrial damage that releases cytochrome c and activates caspase 3.[48,69] Caspase 3, cleaves majority of the cellular substances during the apoptotic process, leading to DNA fragmentation. The other nuclear target is PARP, which plays an important role in the repair of damaged DNA.[70] The triggering of caspase-3 and PARP in the tumour mass is an indicator of tumour cell apoptosis.[71,72] In our study, increases in caspase-3 and PARP immunoreactivities were demonstrated in the tumour masses as treatment-related tumour cell apoptosis, in the order of HePC-NLCs > pure drug >> saline, which corresponded well with the tumour volume data. These results provide direct evidence that the apoptosis-mediated antitumor activities of HePC can be potentiated by its loading into NLCs.

Table 4 Histological Analysis of Pure Drug and HePC-NLCs Applied Tumor Masses Taken Form Female BALB/c Mice

Treatment Group	Tumor Cell Volume ($/mm^2$)	Caspase-3	PARP
Control	85.34 ± 12.46	14.63 ± 3.49	7.83 ± 2.65
Pure Drug	67.45 ± 10.72**	31.17 ± 5.73**	28.34 ± 5.14**
HePC-NLCs	12.79 ± 3.32*	89.18 ±10.37*	89.36 ±9.12*
Normal Saline	82.45 ± 9.93	13.73 ±4.91	8.52 ±3.01

Notes: Each histological value represents the mean ± SD (n=9). Pure drug represent HePC solution. *p <0.01 as compared with control and normal saline treated groups. **p <0.001 as compared with control, pure drug and normal saline treated groups.

Abbreviation: PARP, cleaved poly (ADP-ribose) polymerase.

TUNEL Assay

Additional confirmation of tumour cell apoptosis was acquired using the TUNEL assay, as shown in Figure 9D. DNA fragmentation in the tumour cells was significantly higher in the HePC-NLC-treated mice than in the control mice and pure HePC-treated mice, signifying that enhanced tumour cell death via apoptosis occurred in the NLC-treated group. This could be attributed to internalisation of the NLCs into the tumour tissue because of the targeted drug delivery effect. These results corroborate the histomorphometric results, as demonstrated in Figure 9A–C. Overall, these findings reveal the antitumor potential of HePC, particularly when incorporated into NLCs.

Conclusions

In the present study, HePC-NLCs were prepared using a microemulsion technique. The optimised procedure produced nanoparticles with improved incorporation efficiency. Solid-state characterisation demonstrated transformation of the crystalline drug into an amorphous state. It was observed that HePC-NLCs have the potential to prolong drug release without causing hemolysis in vitro. The enhanced cytotoxicity and uptake of HePC-NLCs in tumour cells showed the antitumor potential of the formulation in vitro. Furthermore, the pharmacokinetic study revealed that the AUC and half-life values were higher for the HePC-NLCs than for the test samples, demonstrating enhanced drug bioavailability of the former. Finally, in vivo antitumor studies confirmed

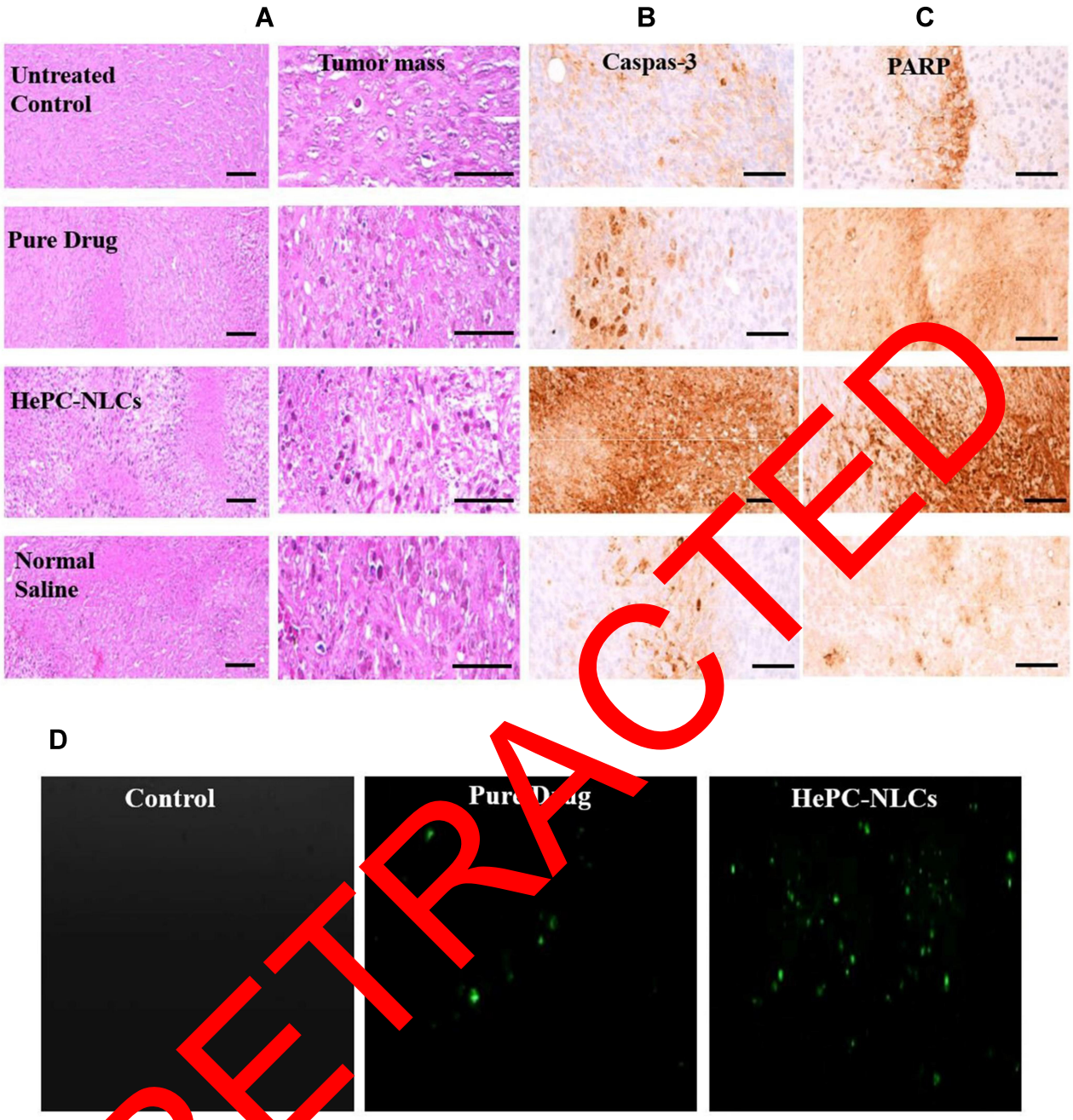

Figure 9 Immu[illegible]histopath[illegible] histopathological alterations in representative tumour masses; immunoreactivity of apoptotic markers (**B**) caspase-3 and (**C**) PARP. (**D**) TUNEL assay [illegible] cells after [illegible]eatment with pure HePC, HePC-NLCs, and saline (control) in vivo. Scale bar = 120 μm.

tumour targeting, internalisation, tumour cell apoptosis, and DNA fragmentation. Thus, the enhanced pharmacokinetic and antitumor potential of the NLCs has been established, particularly when loaded with HePC.

Acknowledgment

The authors are very grateful to the College of Pharmacy, Hanyang University Ansan, South Korea, and Riphah International University Islamabad, Pakistan, for providing some of the reagents and technical support during this project.

Funding

This project was funded by the Higher Education Commission of Pakistan via a grant (No. 21-836/SRGP/R&D/ HEC/2016). Moreover, partial support was provided

by Quaid-i-Azam University, Islamabad, Pakistan through the University Research Fund (URF).

Disclosure

The authors reported no conflicts of interest for this work.

References

1. Freddie Bray JF, Isabelle Soerjomataram RL, Siegel LA, Torre AJ. GLOBOCAN estimates of incidence and mortality worldwide for 36 cancers in 185 countries. *Cancer J Clin*. 2018;68:394–424. doi:10.3322/caac.21492
2. Danker K, Reutter W, Semini G. Glycosidated phospholipids: uncoupling of signalling pathways at the plasma membrane. *Br J Pharmacol*. 2010;160:36–47. doi:10.1111/j.1476-5381.2009.00626.x
3. Thambiraj S, Shruthi S, Vijayalakshmi R, Shankaran DR. Evaluation of cytotoxic activity of docetaxel loaded gold nanoparticles for lung cancer drug delivery. *Cancer Treat Res Commun*. 2019;21:100–157. doi:10.1016/j.ctarc.2019.100157
4. Din F, Choi JY, Kim DW, et al. Irinotecan-encapsulated double-reverse thermosensitive nanocarrier system for rectal administration. *Drug Deliv*. 2017;24:502–510. doi:10.1080/10717544.2016.1272651
5. Cao C, Wang Q, Liu Y. Lung cancer combination therapy: doxorubicin and β-elemene co-loaded, pH-sensitive nanostructured lipid carriers. *Drug Des Devel Ther*. 2019;13:1087. doi:10.2147/DDDT.S198003
6. Xie J, Fan Z, Li Y, et al. Design of pH-sensitive methotrexate prodrug-targeted curcumin nanoparticles for efficient dual-drug delivery and combination cancer therapy. *Int J Nanomedicin*. 2018;13:1381. doi:10.2147/IJN.S152312
7. da Gama Bitencourt JJ, Pazin WM, Ito AS, et al. Miltefosine-loaded lipid nanoparticles: improving miltefosine stability and reducing its hemolytic potential toward erythtocytes and its cytotoxic effect on macrophages. *Biophys Chem*. 2016;2[illegible]20–31. doi:10.1016/j.bpc.2016.07.005
8. Fiegl M, Lindner LH, Juergens M, [illegible] H, Hidd[illegible]ann W, Braess J. Erufosine, a novel alkylphospho[illegible]ne, in acute myeloid leukemia: single activity and combination with other antileukemic drugs. *Cancer Chemother Pharmacol*. 2008;[illegible]321–329. doi:10.1007/s00280-007-0612-7
9. Dorlo TP, Balasegaram M, Beijnen JH, de Vries PJ. Miltefosine: a review of its pharmacology and therapeutic efficacy in the treatment of leishmaniasis. *J Antimicrob Chemother*. 2012;67:2576–2597. doi:10.1093/[illegible]ks275
10. van Blitterswijk WJ, Verheij M. Anticancer alkylphospholipids: mechanisms of action, cellular sensitivity and resistance, and clinical prospects. *Curr Pharm Des*. 2008;14:2061–2074. doi:10.2174/138161208785294636
11. Wieder T, Reutter W, Orfanos CE, Geilen CC. Mechanisms of action of phospholipid analogs as anticancer compounds. *Prog Lipid Res*. 1999;38:249. doi:10.1016/S0163-7827(99)00004-1
12. Kip AE, Schellens JH, Beijnen JH, Dorlo TP. Clinical pharmacokinetics of systemically administered antileishmanial drugs. *Clin Pharmacokinet*. 2018;57:151–176. doi:10.1007/s40262-017-0570-0
13. Chrastina A, Baron VT, Abedinpour P, Rondeau G, Welsh J, Borgström P. Plumbagin-loaded nanoemulsion drug delivery formulation and evaluation of antiproliferative effect on prostate cancer cells. *Biomed Res Int*. 2018;2018. doi:10.1155/2018/9035452
14. Ferreira M, Chaves LL, Lima SAC, Reis S. Optimization of nanostructured lipid carriers loaded with methotrexate: a tool for inflammatory and cancer therapy. *Int J Pharm*. 2015;492:65–72. doi:10.1016/j.ijpharm.2015.07.013
15. Song M, Wang J, Lei J, et al. Preparation and evaluation of liposomes co-loaded with doxorubicin, phospholipase D Inhibitor 5-Fluoro-2-Indolyl Deschlorohalopemide (FIPI) and D-Alpha Tocopheryl Acid Succinate (α-TOS) for anti-metastasis. *Nanoscale Res Lett*. 2019;14(1):1–13. doi:10.1186/s11671-019-2964-4
16. Zeb A, Rana I, Choi H-I, et al. Potential and applications of nanocarriers for efficient delivery of biopharmaceuticals. *Pharmaceutics*. 2020;12:1184. doi:10.3390/pharmaceutics12121184
17. Ud Din F, Kim DW, Choi JY, et al. Irinotecan-loaded double-reversible thermogel with improved antitumor efficacy without initial burst effect and toxicity for intramuscular administration. *Acta Biomater*. 2017;54:239–248. doi:10.1016/j.actbio.2017.03.007
18. Mir M, Ishtiaq S, Rabia S, et al. Nanotechnology: from in vivo imaging system to controlled drug delivery. *Nanoscale Res Lett*. 2017;12:500. doi:10.1186/s11671-017-[illegible]
19. Sabir F, Asad MI, Qindeel M, et al. Polymeric nanogels as versatile nanoplatforms for biomedical applications. *J Nanomater*. 2019;2019:1–16. doi:10.1155/2019/1526186
20. Tran TH, Ramasamy T, Truong DH, et al. Development of vorinostat-loaded solid lipid nanoparticles to enhance pharmacokinetics and efficacy against multidrug-resistant cancer cells. *Pharm Res*. 2014;31(8):19[illegible]1988[illegible]oi:10.1007/s11095-014-1300-z
21. Khan N, Shah FA, Rana I, et al. Nanostructured lipid carriers-mediated brain delivery of carbamazepine for improved in vivo anticonvulsant and anxiolytic activity. *Int J Pharm*. 2020;577:11903[illegible]doi:10.1016/j.ijpharm.2020.119033
22. Agarwal Y, Petkar KC, Sawant KK. Development, evaluation and clinical studies of acitretin loaded nanostructured lipid carriers for topical treatment of psoriasis. *Int J Pharm*. 2010;401(1–2):93–102. doi:10.1016/j.ijpharm.2010.09.007
Fang C-L, Al-Suwayeh S, Fang J-Y. Nanostructured lipid carriers (NLCs) for drug delivery and targeting. *Recent Pat Nanotechnol*. 2013;7(1):41–55. doi:10.2174/187221013804484827
Jaiswal P, Gidwani B, Vyas A. Nanostructured lipid carriers and their current application in targeted drug delivery. *Artif Cells, Nanomed Biotechnol*. 2016;44(1):27–40. doi:10.3109/21691401.2014.909822
25. Ud Din F, Aman W, Ullah I, et al. Effective use of nanocarriers as drug delivery systems for the treatment of selected tumors. *Int J Nanomedicine*. 2017;12:7291. doi:10.2147/IJN.S146315
26. Yhee JY, Son S, Son S, Joo MK, Kwon IC. The EPR effect in cancer therapy. In: Bae Y, Mrsny R, Park K, editors. *Cancer Targeted Drug Delivery*. New York: Springer; 2013:621–632.
27. Maeda H. Research spotlight: emergence of EPR effect theory and development of clinical applications for cancer therapy. *Ther Deliv*. 2014;5(6):627–630. doi:10.4155/tde.14.36
28. Greish K. Enhanced permeability and retention (EPR) effect for anticancer nanomedicine drug targeting. In: Grobmyer S, Moudgil B, editors. *Cancer Nanotechnology Methods in Molecular Biology (Methods and Protocols); Volume 624*. Humana Press; 2010:25–37.
29. Joshi M, Patravale V. Nanostructured lipid carrier (NLC) based gel of celecoxib. *Int J Pharm*. 2008;346(1–2):124–132. doi:10.1016/j.ijpharm.2007.05.060
30. Li Z, Lin X, Yu L, Li X, Geng F, Zheng L. Effects of chloramphenicol on the characterization of solid lipid nanoparticles and nanostructured lipid carriers. *J Dispers Sci Technol*. 2009;30(7):1008–1014. doi:10.1080/01932690802701663
31. Jin SG, Choi H-G. Particle and gel characterization of irinotecan-loaded double-reverse thermosensitive hydrogel. *Polymers*. 2021;13:551. doi:10.3390/polym13040551
32. Ud Din F, Mustapha O, Dw K, et al. Novel dual-reverse thermosensitive solid lipid nanoparticle-loaded hydrogel for rectal administration of flurbiprofen with improved bioavailability and reduced initial burst effect. *Eur J Pharm Biopharm*. 2015;94:64–72. doi:10.1016/j.ejpb.2015.04.019

33. Khan AS, Ud Din F, Ali Z, et al. Development, in vitro and in vivo evaluation of miltefosine loaded nanostructured lipid carriers for the treatment of cutaneous leishmaniasis. *Int J Pharm*. 2020;120109. doi:10.1016/j.ijpharm.2020.120109
34. Ud Din F, Rashid R, Mustapha O, et al. Development of a novel solid lipid nanoparticles-loaded dual-reverse thermosensitive nanomicelle for intramuscular administration with sustained release and reduced toxicity. *RSC Adv*. 2015;5:43687–43694. doi:10.1039/C5RA05656J
35. Mustapha O, Din FU, Kim DW, et al. Novel piroxicam-loaded nanospheres generated by the electrospraying technique: physicochemical characterisation and oral bioavailability evaluation. *J Microencapsul*. 2016;33:323–330. doi:10.1080/02652048.2016.1185475
36. Ud Din F, Zeb A, Shah KU. Development, in-vitro and in-vivo evaluation of ezetimibe-loaded solid lipid nanoparticles and their comparison with marketed product. *J Drug Deliv Sci Technol*. 2019;51:583–590. doi:10.1016/j.jddst.2019.02.026
37. Rizvi SZH, Shah FA, Khan N, et al. Simvastatin-loaded solid lipid nanoparticles for enhanced anti-hyperlipidemic activity in hyperlipidemia animal model. *Int J Pharm*. 2019;560:136–143. doi:10.1016/j.ijpharm.2019.02.002
38. Elmowafy M, Ibrahim HM, Ahmed MA, Shalaby K, Salama A, Hefesha H. Atorvastatin-loaded nanostructured lipid carriers (NLCs): strategy to overcome oral delivery drawbacks. *Drug Deliv*. 2017;24(1):932–941. doi:10.1080/10717544.2017.1337823
39. Wang -J-J, Liu K-S, Sung K, Tsai C-Y, Fang J-Y. Lipid nanoparticles with different oil/fatty ester ratios as carriers of buprenorphine and its prodrugs for injection. *Eur J Pharm Sci*. 2009;38(2):138–146. doi:10.1016/j.ejps.2009.06.008
40. Tran TH, Choi JY, Ramasamy T, et al. Hyaluronic acid-coated solid lipid nanoparticles for targeted delivery of vorinostat to CD44 overexpressing cancer cells. *Carbohydr Polym*. 2014;114:407–415. doi:10.1016/j.carbpol.2014.08.026
41. Seto JE, Polat BE, VanVeller B, Lopez RFV, Langer [illegible] Blankschtein D. Fluorescent penetration enhancers for transderma[illegible] applications. *J Control Release*. 2012;158(1):85–92. doi:10.1016/j.jconrel.2011.10.018
42. Khan MW, Zhao P, Khan A, et al. Synergism of [illegible]splatin-o[illegible]nolic acid co-loaded calcium carbonate nanoparticle[illegible]n hepa[illegible]llular carcinoma cells for enhanced apoptosis and [illegible]educe[illegible]he[illegible]totoxicity. *Int J Nanomedicine*. 2019;14:3753. doi:[illegible]2147/IJN.S[illegible]651
43. Park JH, Cho JH, Kim DS, et al. Reva[illegible]-loaded surfac[illegible]modified solid dispersion: physicochemica[illegible] charac[illegible]zation and [illegible] vivo evaluation. *Pharm Dev Techn*[illegible] 2019;24(6):7[illegible]793. doi:10.1080/10837450.2019.1597114
44. Kim JS, Ud Din F, Le[illegible]SM, et a[illegible]Comparative study between high-pressure homogeni[illegible]ion an[illegible]Shirasu porous glass membrane technique in sildenafil base[illegible]d solid SN[illegible]DDS: effects on physicochemical pr[illegible]and i[illegible]vivo ch[illegible]acteristics. *Int J Pharm*. 2020;592:12[illegible]39.
45. Han B, [illegible]g Y, Ch[illegible] L, et al. Preparation, characterization, and pharmacoki[illegible]c s[illegible]dy of a [illegible]vel long-acting targeted paclitaxel liposome with [illegible]tumor activity. *Int J Nanomedicine*. 2020;15:553. doi:10.2147/IJN.S[illegible]715
46. Barrett KL, Willingh[illegible] JM, Garvin AJ, Willingham MC. Advances in cytochemical methods for detection of apoptosis. *J Histochem Cytochem*. 2001;49(7):821–832. doi:10.1177/002215540104900703
47. Shi S-R, Chaiwun B, Young L, Cote R, Taylor C. Antigen retrieval technique utilizing citrate buffer or urea solution for immunohistochemical demonstration of androgen receptor in formalin-fixed paraffin sections. *J Histochem Cytochem*. 1993;41:1599–1604. doi:10.1177/41.11.7691930
48. Choi JY, Ramasamy T, Tran TH, et al. Systemic delivery of axitinib with nanohybrid liposomal nanoparticles inhibits hypoxic tumor growth. *J Mater Chem B*. 2015;3(3):408–416. doi:10.1039/C4TB01442A
49. Park JC, Lee YJ, Choi HY, Shin YK, Kim JD, Ku SK. In vivo and in vitro antitumor effects of platycodin D, a saponin purified from platycodi radix on the H520 lung cancer cell. *Evid Based Complement Alternat Med*. 2014;2014:1–17. doi:10.1155/2014/478653
50. Jing Y, Zaias J, Duncan R, Russell SJ, Merchan JR. In vivo safety, biodistribution and antitumor effects of uPAR retargeted oncolytic measles virus in syngeneic cancer models. *Gene Ther*. 2014;21(3):289–297. doi:10.1038/gt.2013.84
51. Haider M, Abdin SM, Kamal L, Orive G. Nanostructured lipid carriers for delivery of chemotherapeutics: a review. *Pharmaceutics*. 2020;12(3):288. doi:10.3390/pharmaceutics12030288
52. Beloqui A, Solinís MÁ, Rodríguez-Gascón A, Almeida AJ, Préat V. Nanostructured lipid carriers: promising drug delivery systems for future clinics. *Nanomedicine*. 2016;12(1[illegible]1. doi:10.1016/j.nano.2015.09.004
53. Doktorovová S, Araújo J, Garcia[illegible]L, Rakovský [illegible] Souto EB. Formulating fluticasone propionate [illegible] novel PE[illegible]-containing nanostructured lipid carri[illegible]s (PEG[illegible]LC). *Colloids Surf B Biointerfaces*. [illegible]010;75(2):538–5[illegible] doi:10.1016/j.colsurfb.2009.09.033
54. Shao Z, Shao J, Tan [illegible] et a[illegible]Tar[illegible]ed lung ca[illegible]er therapy: preparation and optimization [illegible]transferri[illegible]corated [illegible]ostructured lipid carriers as novel nano[illegible]cine for co-de[illegible]ry [illegible] anticancer drugs and DNA. *Int J Nano[illegible]dicine*[illegible]015;10:1223. [illegible]:10.2147/IJN.S77837
55. Chanburee S, Tiyaboo[illegible]hai W. Mucoadhesive nanostructured lipid carri[illegible]Cs) as poten[illegible] carriers for improving oral delivery of c[illegible]cumin. *Drug Dev Ind Pharm*. 2017;43(3):432–440. doi:10.1080/[illegible]639045.2016.[illegible]57020
56. [illegible]aleeq N, Din F[illegible] Khan AS, Rabia S, Dar J, Khan GM. Development o[illegible]tosulpiride-l[illegible]ded solid lipid nanoparticles and their in vitro and in viv[illegible]n with commercial product. *J Microencapsul*. 2020;37(2):160–169. doi:10.1080/02652048.2020.1713242
57. [illegible]BA, AbdelMalak NS, Badawi AA. Formulation of a novel oxybenzone-loaded nanostructured lipid carriers (NLCs). *Aaps Pharmscitech*. 2010;11:1684–1694. doi:10.1208/s12249-010-9553-2
58. Souto E, Wissing S, Barbosa C, Müller R. Development of a controlled release formulation based on SLN and NLC for topical clotrimazole delivery. *Int J Pharm*. 2004;278(1):71–77. doi:10.1016/j.ijpharm.2004.02.032
59. Üner M. Preparation, characterization and physico-chemical properties of solid lipid nanoparticles (SLN) and nanostructured lipid carriers (NLC): their benefits as colloidal drug carrier systems. *Pharmazie*. 2006;61:375–386.
60. Tamjidi F, Shahedi M, Varshosaz J, Nasirpour A. Nanostructured lipid carriers (NLC): a potential delivery system for bioactive food molecules. *Innov Food Sci Emerg Technol*. 2013;19:29–43. doi:10.1016/j.ifset.2013.03.002
61. Das S, Khan W, Mohsin S, Kumar N. Miltefosine loaded albumin microparticles for treatment of visceral leishmaniasis: formulation development and in vitro evaluation. *Polym Adv Technol*. 2011;22(1):172–179. doi:10.1002/pat.1710
62. Kaufmann-Kolle P, Drevs J, Berger M, et al. Pharmacokinetic behavior and antineoplastic activity of liposomal hexadecylphosphocholine. *Cancer Chemother Pharmacol*. 1994;34:393–398. doi:10.1007/BF00685563
63. Petersen S, Steiniger F, Fischer D, Fahr A, Bunjes H. The physical state of lipid nanoparticles influences their effect on in vitro cell viability. *Eur J Pharm Biopharm*. 2011;79(1):150–161. doi:10.1016/j.ejpb.2011.03.022
64. Chinsriwongkul A, Chareanputtakhun P, Ngawhirunpat P, et al. Nanostructured Lipid Carriers (NLC) for parenteral delivery of an anticancer drug. *AAPS PharmSciTech*. 2012;13(1):150–158. doi:10.1208/s12249-011-9733-8

65. Peer D, Karp JM, Hong S, Farokhzad OC, Margalit R, Langer R. Nanocarriers as an emerging platform for cancer therapy. *Nat Nanotechnol*. 2007;2(12):751–760. doi:10.1038/nnano.2007.387
66. Manchun S, Dass CR, Cheewatanakornkool K, Sriamornsak P. Enhanced anti-tumor effect of pH-responsive dextrin nanogels delivering doxorubicin on colorectal cancer. *Carbohydr Polym*. 2015;126:222–230. doi:10.1016/j.carbpol.2015.03.018
67. Ramasamy T, Choi JY, Cho HJ, et al. Polypeptide-based micelles for delivery of irinotecan: physicochemical and in vivo characterization. *Pharm Res*. 2015;32(6):1947–1956. doi:10.1007/s11095-014-1588-8
68. Kim J-Y, Kim J-K, Park J-S, Byun Y, Kim C-K. The use of PEGylated liposomes to prolong circulation lifetimes of tissue plasminogen activator. *Biomaterials*. 2009;30(29):5751–5756. doi:10.1016/j.biomaterials.2009.07.021
69. Hua P, Liu J, Tao J, Liu J, Yang S. Influence of caspase-3 silencing on the proliferation and apoptosis of rat bone marrow mesenchymal stem cells under hypoxia. *Int J Clin Exp Med*. 2015;8:1624.
70. Smyth PG, Berman SA, Bursztajn S. Markers of apoptosis: methods for elucidating the mechanism of apoptotic cell death from the nervous system. *Biotechniques*. 2002;32(3):648–665. doi:10.2144/02323dd02
71. Qin Y, Sun C-Y, Lu F-R, et al. Cardamonin exerts potent activity against multiple myeloma through blockade of NF-κB pathway in vitro. *Leuk Res*. 2012;36(4):514–520. doi:10.1016/j.leukres.2011.11.014
72. Fang EF, Zhang CZY, Zhang L, et al. Trichosanthin inhibits breast cancer cell proliferation in both cell lines and nude mice by promotion of apoptosis. *PLoS One*. 2012;7(9):e41592. doi:10.1371/journal.pone.0041592